JOURNAL OF MATERIALS SCIENCE **34** (1999) 5337–5342

Study of the low stress plasticity in single-crystal MgO by nanoindentation and atomic force microscopy

C. TROMAS, J. C. GIRARD, V. AUDURIER, J. WOIRGARD
Laboratoire de Métallurgie Physique, U.M.R. 6630, SP2MI, Bd. 3 Téléport 2, B.P. 174, 86960 FUTUROSCOPE Cedex
E-mail: CHRISTOPHE.TROMAS@LMP.UNIV-POITIERS.FR.

Berkovich nanoindentations have been performed at ambient temperature with a new apparatus on (001) cleaved surfaces of single-crystal Magnesium Oxide (MgO). Rosette slip lines pattern has been observed at a nanometric scale by Atomic Force Microscope. Moreover, the load-displacement curves present particular features such as pop-in, which has been linked to the AFM surface topography observations. Finally, we show that the combination of a new nanoindentation apparatus and an Atomic Force Microscope allows to study the very early stages of the plastic deformation during a nanoindentation in terms of individual dislocations.

1. Introduction

The nanoindentation test is usually used not only to measure the mechanical properties of materials, such as the hardness or the Young modulus, but also to study the early stages of plasticity at the nanometer level, despite the fact that the stress and strain distribution associated with indentations is still poorly understood, especially in crystalline solids exhibiting well-defined slip systems.

The aim of this work is thus to contribute to the understanding of the dislocation mechanisms involved in the deformation of single-crystal MgO under very low stress. The choice of the material was dictated by the fact that the plastic zones surrounding indentions have been extensively studied, by various observation techniques such as, optical microscopy [1, 2], scanning tunneling microscopy (STM) [3], or scanning electron microscopy (SEM) [4, 5]. Some special features, such as rosettes arms [6, 7], have been observed but most of these studies were conducted by microindentation, at load levels too high to allow precise observations of the surface at the very beginning of the deformation process.

The purpose of the present work was, therefore, to observe by Atomic Force Microscopy, the fine details of the surface around low load Berkovich nanoindentations performed on MgO crystals {001} planes. The plastic deformation has been limited to its very early stages thanks to the precision offered by the nanoindentation test [8]. The precision of the AFM allowed the observation of the topography of the indented area at a nanometric scale.

2. Experimental results

Single-crystals MgO were cleaved along {100} planes. AFM observations were performed with a Digital Instrument Nanoscope III apparatus. The freshly cleaved surfaces exhibit numerous steps with heights ranging from a few hundreds of nanometres down to the monolayer thickness, as previously observed by Sangwal *et al*. [9]. Nanoindentations were performed on wide {100} terraces, separated by macroscopic steps. Preliminary AFM studies had revealed disc-like islands attributed to hydroxyl and carboxylate groups [10]. Due to this contamination, indentations and AFM observations were restricted to a lapse of time of a few hours after cleavage. Moreover, AFM images were performed in tapping mode to avoid friction and subsequent contamination that would occur in contact mode.

Nanoindentations were performed with a home-built nanoindentation apparatus [8]. Thermal drifts are drastically reduced in particular, by making the measurement head in a low expansion material, for the measurement head, and applying the indentation force electrostatically. Thanks to a special design, a very low frame compliance is obtained given that the specimens are properly mounted. The unloading period, 12 s, has been taken shorter than the loading one, 60 s, to avoid creep or delayed plasticity effects.

Variable load indentations were located 10 microns apart, to prevent overlapping of the plastified zones, forming a $100 \times 100\ \mu m^2$ arrays limited by large indents (80 mN) 15 μm appart, defining two easily visible orthogonal axes. The difficulty to obtain AFM images of the indents, fastly enough to avoid contamination, is

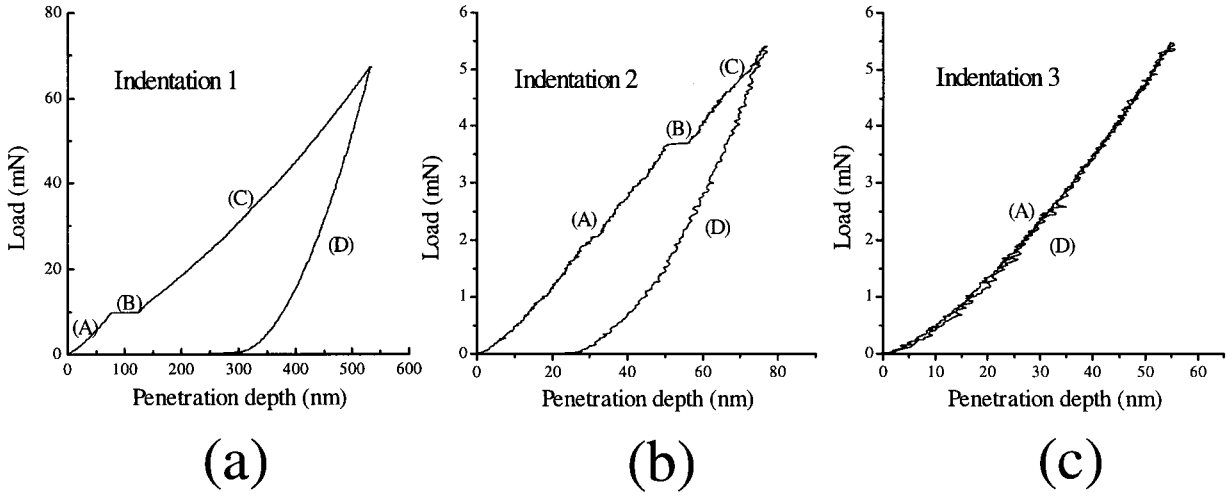

Figure 1 Load-displacement curves of three load controlled Berkovich nanoindentations for respectively: (a) 67 mN, (b) 5.5 mN, and (c) 5.5 mN applied load. Four different stages may be observed on these curves: A: Elastic deformation, B: Pop-in, C: Elasto-plastic deformation, D: Elastic unloading.

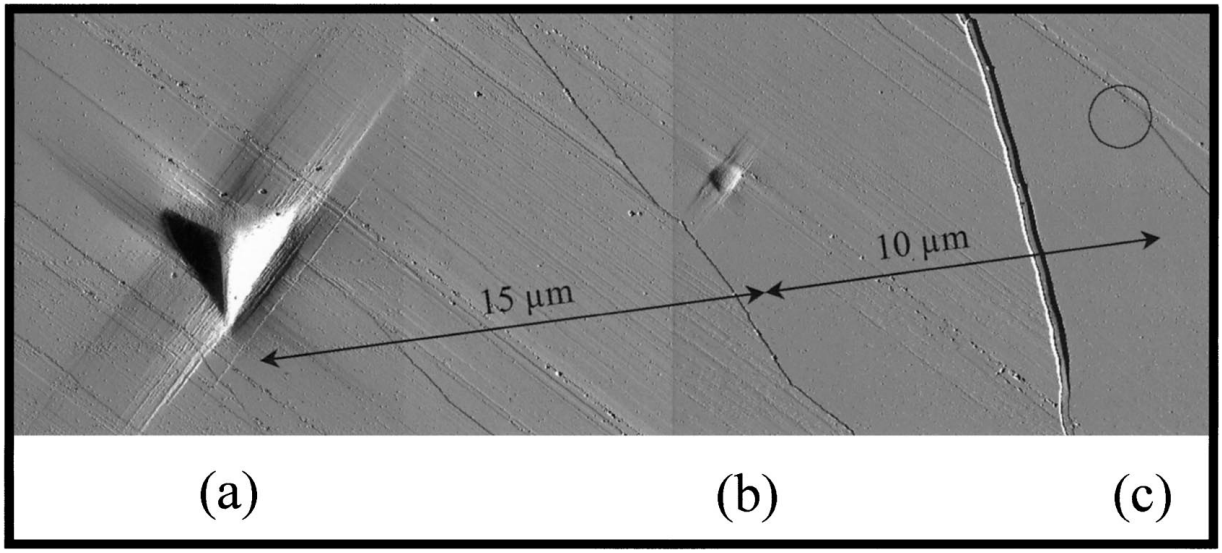

Figure 2 Atomic Force Microscope amplitude signal image (tapping mode) of the three previous indentations.

due to the fact that the indents, even the largest ones, cannot be observed with the optics mounted on the AFM. Thus, in a first step, the largest indents are located, with a powerful optical microscope, in respect to macroscopic surface defects that can be latter detected with the X400 optical system connected to the AFM.

It was thus possible to identify individual indentations and to link them to the corresponding load-displacement curves. The selected ($15 \times 15\ \mu m^2$) areas were then imaged by the Atomic Force Microscope with a nanometric resolution.

3. Experiments

Typical load-displacement curves are plotted in Fig. 1a, b, and c and the corresponding AFM images of the residual indents in Fig. 2a, b and c. As shown in Fig. 1a, loading starts with an elastic deformation (A), followed by a fast increase in penetration at constant load (B). That kind of accident is generally called a "pop-in," and has already been observed in different materials, such as GaAs [11], Fe-Si [12], W [13] and Au [14]. Loading goes on with an elasto-plastic behaviour (C). Finally tests end with quasi-elastic unloading (D).

The Young's modulus obtained from the nanoindentation tests (312 GPa) is in a good agreement with tabulated values. The hardness is plotted in Fig. 3 as a function of the computed true penetration depth h_c [15]. It can be seen that in the part (a) of this curve, the

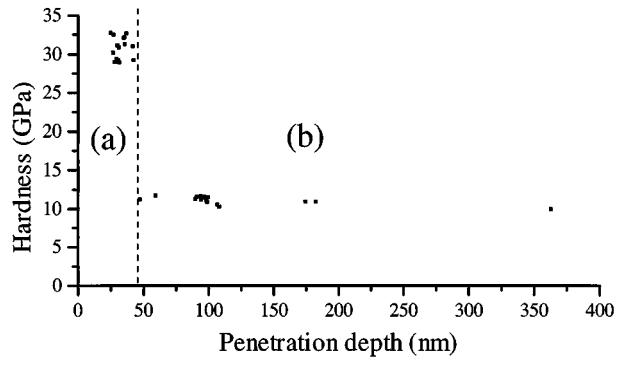

Figure 3 Hardness-maximum penetration curve. The hardness falls down from 30 GPa (part (a))to 12 GPa (part (b)) at the maximum penetration depth corresponding to the pop-in apparition.

hardness reaches a very high value (30 GPa), and then, in the part (b), falls down to a lower constant value (12 GPa). It will be shown that the transition between parts (a) and (b) corresponds to the pop-in phenomenon linked with dislocations nucleation.

To study the pop-in phenomenon, the three indents corresponding to Fig. 1a, b and c, obtained at high and low loads, have been observed by AFM (Fig. 2a, b and c). At the highest load (Figs 1a and 2a), the load-displacement curve presents a "pop-in" and a residual penetration in agreement with the depth of the residual indent observed by AFM. The low load indents of Figs 1b–2b and 1c–2c, performed at the same load, either exhibits a pop-in and a residual displacement, or no pop-in and no residual deformation. In the later case (Figs 1c and 2c), an elastic penetration as high as 50 nm being observed. From this experiment, the pop-in phenomenon has been clearly correlated with the initiation of an irreversible deformation, in agreement with the earlier results of Gerberich *et al*. [16].

4. Atomic force microscopy observations

A 75 mN load indentation observed by AFM is shown in a three dimensional representation (Fig. 4) or in an amplitude image (Fig. 5). A 315 nm remaining depth is measured by AFM for this indentation. The triangular shape of the residual inprint reflects that of the three sided pyramidal Berkovich indentor.

In addition to parallel cleavage steps, the AFM images in Figs 4 and 5 reveal a very specific surface relief: a four arms pattern centred on the indent, known as a rosette. The surface topography of these rosette arms was observed in MgO by Armstrong and Wu [5] with microindentations. These U shaped arms are depressed troughs extending along ⟨100⟩ directions and gently sloping up to the surface. An important upward displacement is also visible, in Fig. 4, at the corners of the four intersecting rosette arms. In Fig. 5 it can also be seen that, in agreement with Hammond and Armstrong [17], the indentation edges slightly bow-out horizontally.

In addition to SEM studies, AFM offers a new insight to the fine structure of surface deformations, allowing rosette arms to be analysed in term of elementary steps parallel to ⟨100⟩ directions, associated with the emergence of dislocations. The height of the steps corresponds to the Burgers vector component perpendicular to the surface. The step density is higher at the edge of the arms, the central part remaining flat. Furthermore, a second system of ⟨100⟩ direction slip lines, corresponding to an additional deformation mechanism, perpendicularly intersects the rosette arms. Only a few of these slip lines are seen around the nanoindent. This has to be compared with the previous SEM observations of Armstrong and Wu [5], or optical observations of Keh *et al*. [18], around large Vickers microindents (3N load).

The 8 mN indent shown in Fig. 6 is one of the smallest residual deformation that has been observed and corresponds to the early stages of the various deformation features already described for the 75 mN indentation. As this indent corresponds to the first stages of the irreversible deformation, the individual steps of the rosette arms are clearly resolved, as it can be seen in the Fig. 7 which represents a cross section of one of the rosette arms.

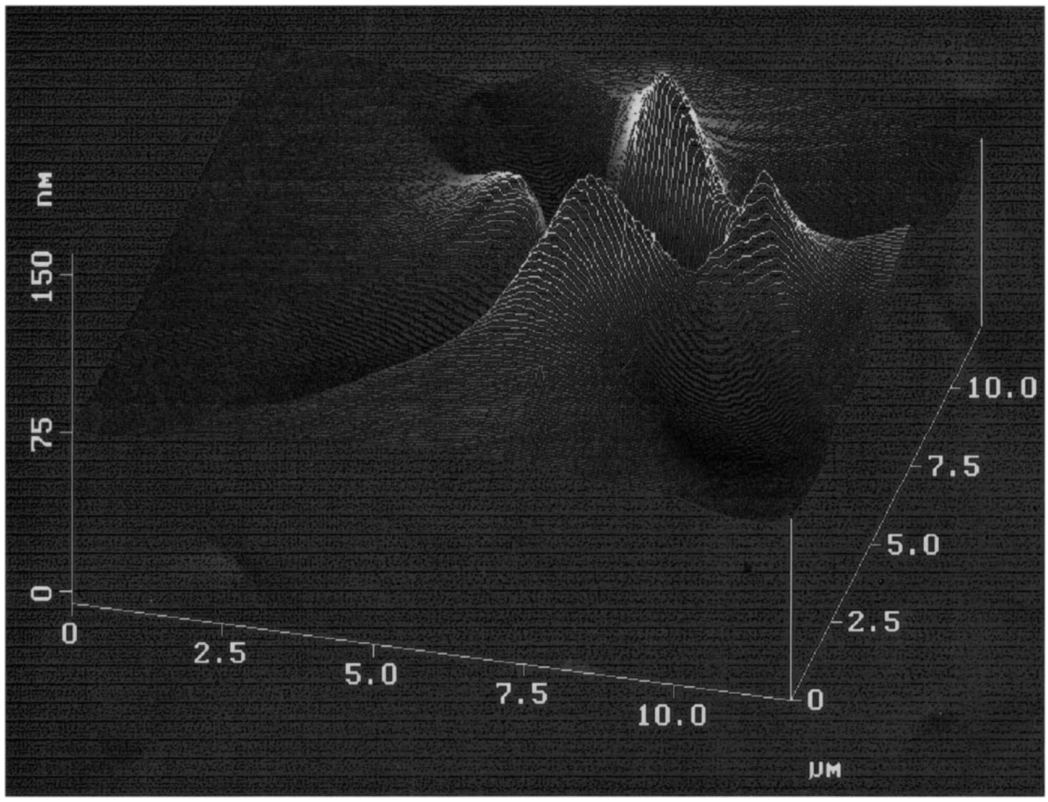

Figure 4 Atomic Force Microscope height signal image (tapping mode) of a 75 mN load controlled indentation, in 3D view.

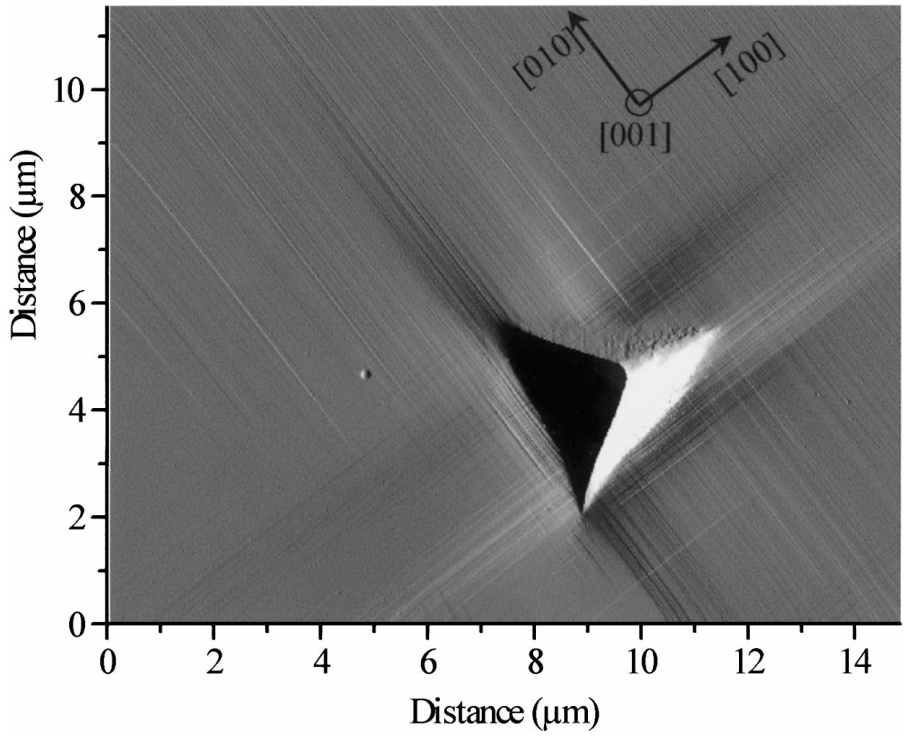

Figure 5 Atomic Force Microscope amplitude signal image (tapping mode) of the same indentation as in Fig. 4.

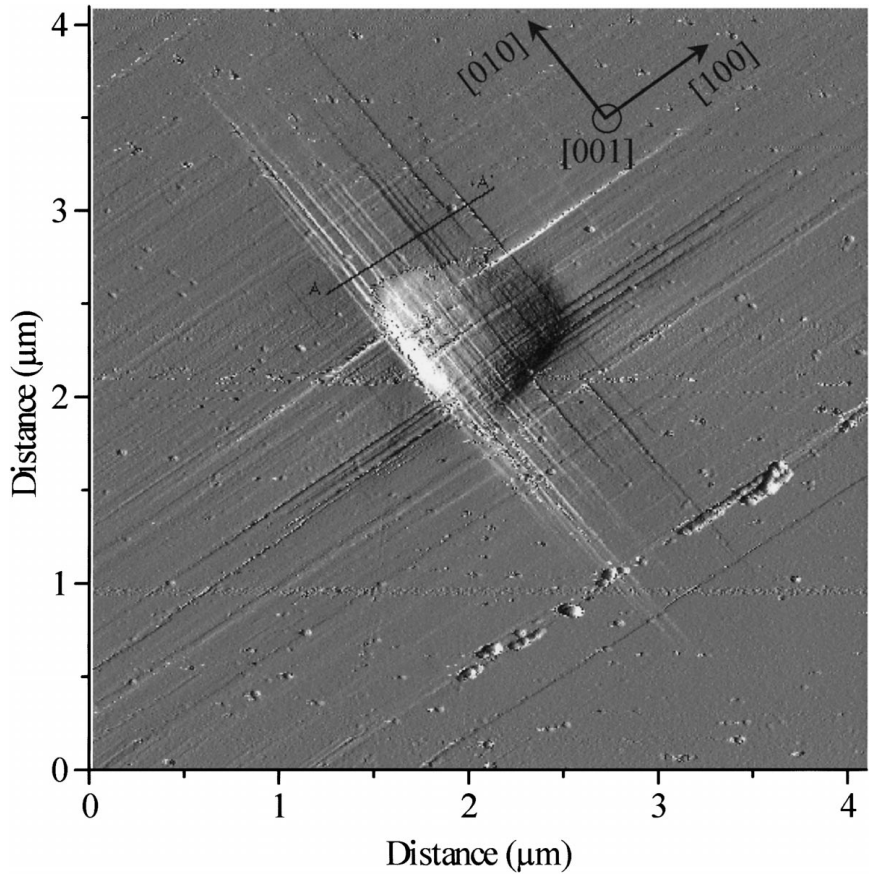

Figure 6 Atomic Force Microscope amplitude signal image (tapping mode) of 8 mN load controlled indentation. Rosette arms slip lines are clearly visible.

The steps forming the rosette arms, which appear as straight lines in the signal error mode AFM image, extend inside the indent, showing that two opposite arms develop simultaneously. It can also be seen that the centre of the indent, in Fig. 6, presents an unsheared 140×140 nm^2 square shaped bottom, corresponding to the crossing of the rosette arms flat bottoms.

Fig. 8 shows the load-displacement curve of the previous 8 mN indentation. Each stage of the curve can be qualitatively and quantitatively correlated with the

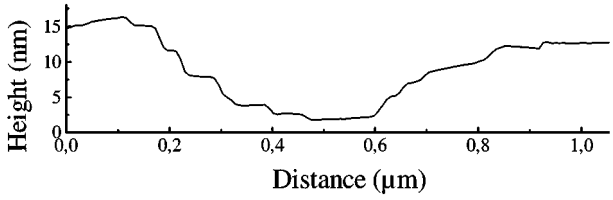

Figure 7 Section AA' of one of the depressed rosette arms of the indent presented in Fig. 6. This section reveals a step profile.

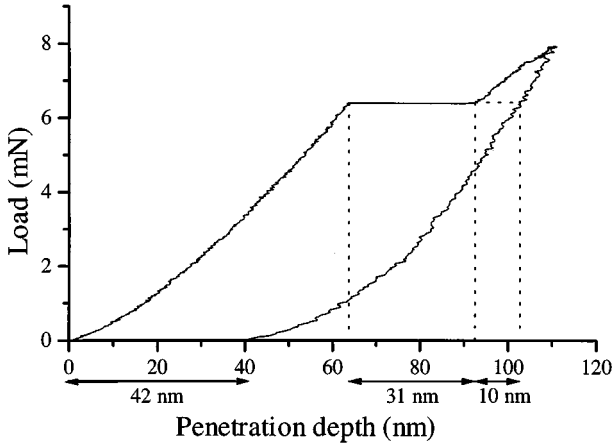

Figure 8 Load-displacement curve corresponding to the indent presented in Fig. 5. This curve shows a large pop-in during the load.

surface topography observed by AFM. At first, the total remaining depth penetration, 42 nm, deduced from the curve agrees with the 41 nm indent depth measured by AFM. Moreover, the curve shows a 10 nm residual penetration after the pop-in, which can be linked to the rosette arm depth measured by AFM just around the indent, that is outside of the two orthogonal other rosette arms. The correspondence between these two measurements indicates that the second regime of indentation, just after the pop-in, corresponds to the rosette arms formation. Moreover, the 31 nm amplitude of the pop-in added to the 10 nm rosette arms depth is exactly the depth of the indent, either measured on the indentation curve or by AFM. From these observations, the pop-in appears as an entirely plastic deformation process. To sum up, the pop-in, corresponding to a sudden and strictly plastic punching, is the first stage of the plastic deformation process. It is followed by an elasto-plastic process responsible for the rosette arms formation.

5. Discussion

As shown in Fig. 1a and b, the first stage of the plastic deformation is quasi-instantaneous. Actually, the indentor punches its shape into the material during the pop-in, by nucleating interstitial dislocation loops with a[100] Burgers vector, as shown schematically in Fig. 9, and previously described by Le Bourhis *et al.* [19], where $a = 4.21$ Å is the lattice parameter of MgO. Once the theoretical elastic limit is reached, a first dislocation loop nucleates, producing a stress relaxation in the material beneath the indentor, the load being thus mostly applied on the limit contact curve between the indentor and the sample surface. A new dislocation loop can immediately nucleate under this curve at a constant load.

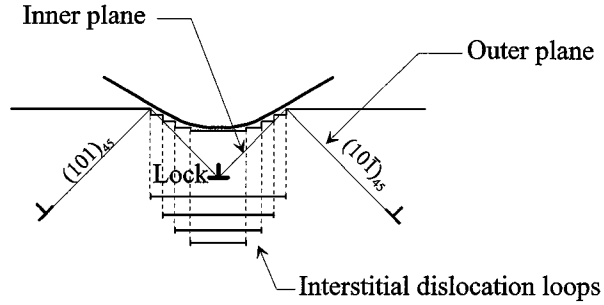

Figure 9 Nucleation of interstitial dislocation loops during the pop-in.

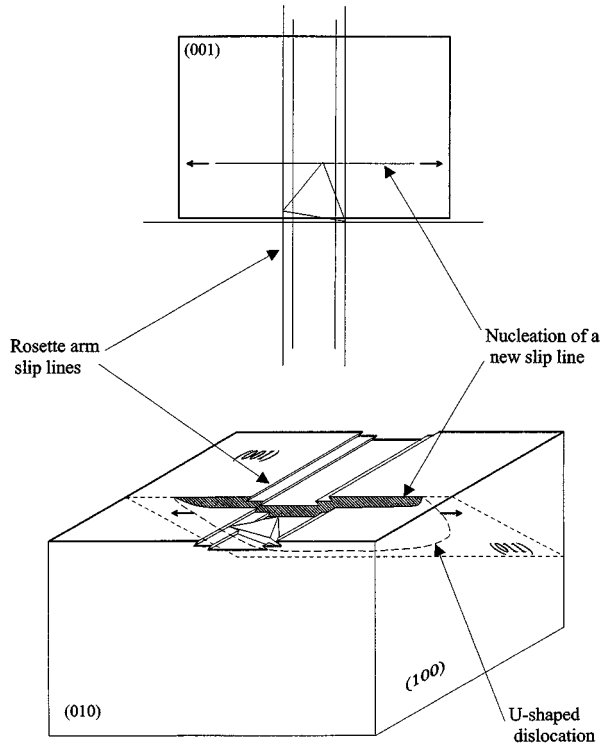

Figure 10 Nucleation of U-shaped dislocation : formation of the rosette slip line pattern.

A catastrophic mechanism is thus initiated. The previously nucleated dislocation loops are repelled deeper into the material until a pill up equilibrium is established. After the pop-in, when the applied stress exceeds the back stress due to the array of prismatic loops, the deformation goes on into {110} planes oriented at 45° relative to the surface. This further mechanism, appearing in Fig. 10, has been associated with the formation of the depressed rosette arms. These $\{110\}_{45}$ planes belong to the $\{110\}\langle 110\rangle$ primary slip system of MgO. One can define $\{110\}_{45}$ inner planes located under the indentor, in opposition to $\{110\}_{45}$ outer plane, as seen in Fig. 9. When the back stress impedes new nucleation under the indentor, dislocations nucleate in the $\{110\}_{45}$ plane starting at the limit contact curve between the indentor and the sample. The extension of rosette arms is essentially controlled by U-shaped dislocations nucleating in the $\{110\}_{45}$ outer planes containing the $\langle 100\rangle$ tangents of the projected contact surface, since gliding in the inner planes may lead to work hardening by formation of Lomer Cottrell locks. During the indentation, the observed steps (Figs 6 and 7) which result of the U-shaped dislocations surface propagation, extend

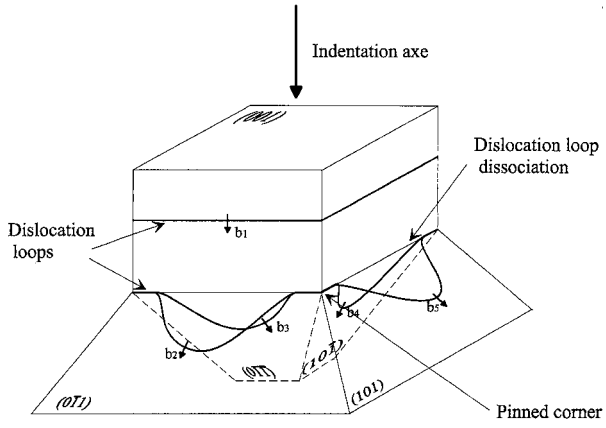

Figure 11 Activation of a third mechanism. The dislocation loops previously nucleated during the pop-in dissociate in $\{011\}_{45}$ planes.

in the $\langle 100 \rangle$ opposite arms, on both sides of the indented area.

As the indentor penetrates deeper into the sample, the contact surface area extends and the active deformation goes on into the following $\{110\}_{45}$ planes. New steps, with an increasing length and parallel to the freezed initial ones, are created outside of the already formed rosette troughs. The resulting step distribution leads to rosette bottom sloping gently up to the surface. It may be observed that the first steps nucleate at the edge of the non sheared square produced during the pop-in. Consequently, the size of the last interstitial loop nucleated during the pop-in can be deduced from the width of the flat bottom of the rosette arms. In the case of the 8 mN load indent presented in Fig. 6, this size is about $140 \times 140\,\text{nm}^2$. The two previous mechanisms can explain the whole features of the low load indents, but not the features associated to the high load indentations.

A third mechanism must be activated. In fact, the interstitial dislocation loops nucleated during the pop-in are unstable in MgO, so they tend to adopt a rectangular shape, in order to dissociate in $\{110\}_{45}$ planes, as shown in Fig. 10. The reaction of dissociation is:

$$a[00\bar{1}] \rightarrow \frac{a}{2}[01\bar{1}] + \frac{a}{2}[0\bar{1}\bar{1}]$$

Upon dissociation, the dislocations are glissile in the $\{110\}_{45}$ planes. Pinned on the corners of their initial rectangles, these dislocation segments act as Frank Read sources. The activation of these Frank Read sources should be taken into account for further deformation under higher load. Moreover, loops emitted by Frank Read sources slip in the $\{110\}_{45}$ planes until they reach the surface and produce new steps along the $\langle 100 \rangle$ directions. From simple geometrical arguments, it is obvious that they reproduce a magnified image of the (001) initial rectangle.

We observed in the experimental results section that these steps appeared only for the highest load indentations, above a critical load, and that their density was correlated to the applied load.

6. Conclusion

During Berkovich nanoindentation tests on (001) surfaces of single-crystal MgO, dislocations nucleate under the contact area between the sample and the indentor because of the high local strain. Three successive deformation mechanisms were taken into account. At the beginning of the irreversible deformation, interstitial dislocation loops nucleate. This event correspond to a pop-in in the indentation load-displacement curve. When the back stress induced by the dislocation loops pill up reaches a given value, a second mechanism starts at the edges of the already formed imprint. U-shaped dislocations nucleate and propagate in $\langle 100 \rangle$ crystallographic directions. This propagation has been characterised by parallel steps on the surface, responsible for the formation of the rosette arms pattern. In the last step, the dislocation loops, previously nucleated, dissociate to act as Frank Read sources in the $\{110\}_{45}$ planes. When the loops emitted from these sources reach the surface, a step pattern appears, reproducing a magnified image of the initial undissociated dislocation loops.

So, the plastic behaviour of an indented single-crystal MgO has been studied in its very early stages by the AFM observation of slip traces on the surface and the analyse of the corresponding indentation load-displacement curves. The combined use of an AFM and a new nanoindentation apparatus allowed the analyse of the plastic deformation in terms of individual dislocations.

References

1. A. S. KEH, *J. Appl. Phys.* **31** (1960) 1538.
2. J. L. LOUBET, J. M. GEORGES, O. MARCHESINI and G. MEILLE, *J. Lub. Techno.* **106** (1984) 43.
3. M. R. CASTELL, M. G. WALLS and A. HOWIE, *Ultramicroscopy* **42–44** (1992) 1490.
4. N. KHASGIWALE and H. M. CHAN, *J. Amer. Ceram. Soc.* **75** (1992) 1924.
5. R. W. ARMSTRONG and C. CM. WU, *ibid.* **61** (1978) 102.
6. H. HARADA and K. SUMINO, *J. Appl. Phys* **53** (1992) 4838.
7. J. DOERSCHEL, *Zeitschrift für Kristallographie* **209** (1994) 210.
8. J. WOIRGARD and J. C. DARGENTON, *Meas. Sci. Technol.* **6** (1995) 16.
9. K. SANGWAL, F. SANZ, J. SERVAT and P. GOROSTIZA, *Surf. Sci.* **383** (1997) 78.
10. D. ABRIOU, F. CREUZET and J. JUPILLE, *ibid.* **352–354** (1996) 499.
11. A. B. MANN and J. B. PETHICA, *Mat Res. Symp.* **436** (1997) 153.
12. W. W. GERBERICH, S. K. VENKATARAMAN, H. HUANG, S. E. HARVEY and D. L. KOHLSTEDT, *Acta Metall. Mater.* **43–44** (1995) 1569.
13. S. A. SYED ASIF and J. B. PETHICA, *Phil. Mag. A* **76** (1997) 1105.
14. J. E. HOUSTON and T. A. MICHALSKE, *Mat. Res. Soc. Symp. Proc.* **436** (1997) 3.
15. J. WOIRGARD and J. C. DARGENTON, *J. of Mat. Res.* **12–9** (1997) 2455.
16. W. W. GERBERICH, J. C. NELSON, E. T. LILLEODDEN, P. ANDERSON and J. T. WYROBECK, *Acta Mater.* **44** (1996) 3585.
17. B. L. HAMMOND and R. W. ARMSTRONG, *Phil. Mag. Let.* **57** (1988) 41.
18. A. S. KEH, J. C. M. LI and Y. T. CHOU, *Acta Met.* **7** (1959) 694.
19. E. LE BOURHIS, J. P. RIVIERE and A. ZOZIME, *J. Mater. Sci.* **31** (1996) 6571.

Received 19 January 1998
and accepted 13 January 1999